Structural anomalies at the ferromagnetic transition and precursor effects in the vicinity of the structural phase transition of $La_{0.815}Ba_{0.185}MnO_3$

Nicola Rotiroti,[1] Sander van Smaalen,[1,*] Rafael Tamazyan,[1,2] and Ya. Mukovskii[3]
[1]*Laboratory of Crystallography, University of Bayreuth, D-95440 Bayreuth, Germany*
[2]*Molecule Structure Research Center, National Academy of Science Ra, Azatutyan avenue 26, 375014 Yerevan, Armenia*
[3]*Moscow State Steel and Alloys Institute, 119049 Moscow, Russian Federation*
(Received 2 March 2006; revised manuscript received 7 August 2006; published 29 September 2006)

Rhombohedral $La_{0.815}Ba_{0.185}MnO_3$ undergoes a phase transition at $T_c=251$ K from a paramagnetic insulating state (PMI) toward a ferromagnetic metallic state (FMM) on cooling. At $T_S=187.1(3)$ K a first-order phase transition occurs toward a structure with monoclinic symmetry. Accurate crystal structures are reported for selected temperatures between T_S and room temperature. Thermal expansion is found to be different in the PMI and FMM phases, with a larger thermal expansion coefficient in the FMM phase. This feature is related to incoherent distortions of the MnO_6 octahedral groups, which are smaller in the FMM state than in the PMI state. Precursor effects are observed as anomalous structural behavior within the rhombohedral phase close to T_S. They indicate two independent contributions to the driving force for the structural transition. Shear distortions of MnO_6 octahedra in the rhombohedral structure are transformed into energetically more stable Jahn-Teller-type distortions in the monoclinic structure. And the larger number of degrees of freedom in monoclinic symmetry allows an energetically more stable coordination of La by oxygen in the monoclinic structure.

DOI: 10.1103/PhysRevB.74.104423 PACS number(s): 61.66.Fn, 75.30.Kz, 61.50.Ks, 61.72.Mm

I. INTRODUCTION

$La_{1-x}Ba_xMnO_3$ manganites are of interest since colossal magnetoresistance (CMR) was observed for this class of compounds.[1,2] Depending on x and the temperature they display different crystal structures as well as different magnetic and transport properties. Powder neutron-diffraction was adopted by Dabrowski *et al.*[3] to investigate $La_{1-x}Ba_xMnO_3$ of compositions $x=0.10-0.24$ at room temperature. They found orthorhombic symmetry *Pbnm* for $x=0.10$ and rhombohedral $R\bar{3}c$ symmetry for $x=0.14-0.24$ while the compound with $x=0.12$ contained both phases; thus, the structural orthorhombic to rhombohedral transition appears for $x=0.13$ at room temperature. The temperature dependence of the lattice parameters of $La_{0.8}Ba_{0.2}MnO_3$ was reported by Arkhipov *et al.*[4] They indexed x-ray powder diffraction diagrams by orthorhombic symmetry *Pbnm* in the range of temperatures $T=80-185$ K, and by rhombohedral symmetry $R\bar{3}c$ for $T\geqslant 185$ K. The two phases coexist between 185 K and 196 K. Employing single-crystal X-ray diffraction, we have confirmed the rhombohedral phase of $La_{0.815}Ba_{0.185}MnO_3$, but for the low-temperature phase we have found a monoclinic structure with $I2/c$ symmetry below the first-order phase transition at $T_c=187.1(3)$ K.[5] Monoclinic $I2/c$ symmetry was also found for $La_{0.788}Sr_{0.212}Mn_{0.958}O_3$.[6] Both the monoclinic $I2/c$ and the orthorhombic *Pbnm* structures are described on a $\sqrt{2}a_c\times\sqrt{2}a_c\times 2a_c$ superlattice of the primitive cubic perovskite-type structure with lattice parameter $a_c\approx 3.9$ Å. An analysis restricted to the determination of the geometries of the lattices is not sufficient to discriminate between the two types of superstructures, and single-crystal diffraction appeared to be essential to discriminate between the two symmetries.

It is known that for the family of compounds $La_{1-x}M_xMnO_3$ (M=Ca, Ba, and Sr; $0.1\leqslant x\leqslant 0.5$), also called La manganites, the CMR effect, and the metal-insulator transition take place in the vicinity of the ferromagnetic phase transition. In the case of $La_{1-x}Ba_xMnO_3$ with nominal composition $x=0.20$ a magnetic phase transition has been observed within the rhombohedral phase from a paramagnetic insulating (PMI) state at high temperatures toward a ferromagnetic metallic (FMM) state at low temperatures. The transition temperature was determined from measurements of the magnetization as $T_c\approx 251$ K on material of the same batch as studied here.[4] Measurements of the magnetization and the electrical resistivity have been reported by Dabrowski *et al.*[3] for ceramic samples of La and Ba manganites with compositions $0.10\leq x\leq 0.24$. Both magnetic and electrical properties lead to equal values for the transition temperatures, with $T_c=261$ K for a sample with $x=0.18$. Ju *et al.* have proposed an (x,T) phase diagram for $La_{1-x}Ba_xMnO_3$ in the range $0\leqslant x\leqslant 1$. They observed a transition at $T_c\approx 275$ K from a PMI state to a ferromagnetic insulating (FMI) state for a composition $x=0.19$ with rhombohedral symmetry.[7] More recently a phase diagram has been given by Zhang *et al.*[8] for thin films and bulk material of $La_{1-x}Ba_xMnO_3$ with compositions $0.05<x<0.33$. They reported $T_c\approx 280$ K for the PMI to FMM transition of a sample of composition $x=0.2$.

It is interesting to note that a correlation was observed between magnetic and electronic phase transitions and variations of crystal structures for similar compounds in the La manganite system. Anomalies in the temperature dependencies of several structural parameters have been reported to be present near the transition temperatures of the magnetic phase transitions in La manganite with orthorhombic structures (space group *Pbnm*), like $La_{1-x}Ca_xMnO_3$ with $0<x\leq 0.33$ and $x=0.5$ and $La_{1-x}Sr_xMnO_3$ with $0.1\leq x\leq 0.2$.[9–14] Furthermore structural variations at the magnetic phase transition were reported for rhombohedral $La_{0.815}Sr_{0.185}MnO_3$.[14]

Rhombohedral $La_{1-x}Ba_xMnO_3$ has been studied so far only by x-ray and neutron powder diffraction, and structural

refinements have not been reported. In order to be able to detect small structural changes, high accuracy is required, which is achieved by x-ray single-crystal diffraction, collecting extensive intensity data sets. Here we report the results of a study of the temperature dependence of the crystal structures of $La_{1-x}Ba_xMnO_3$ ($x=0.185$) in the rhombohedral phase for $188.9 \leq T \leq 295$ K, by single-crystal x-ray diffraction. Structural variations and their correlation with the magnetic phase transition are discussed. Moreover, precursor effects within the rhombohedral phase have been found on approach of the structural phase transition at $T_S = 187.1(3)$ K.

II. EXPERIMENT

Single-crystalline material of nominal composition $La_{0.8}Ba_{0.2}MnO_3$ was grown by the noncrucible floating zone technique.[15] Chemical analysis was conducted by electron microprobe at the Bayerisches Geoinstitut in Bayreuth (D. Krauße), resulting in a La:Ba:Mn ratio of 0.815(10):0.185(6):0.996(8). A smaller concentration of Ba in the sample than that given by the nominal composition can be explained by high, selective evaporation of barium from the melt. A piece of about $0.13 \times 0.06 \times 0.05$ mm^3 was cut from the crystalline material and used for low-temperature single-crystal x-ray diffraction on a Nonius MACH3 diffractometer, equipped with a rotating anode generator and a graphite monochromator (Mo $K\alpha$ radiation of wavelength 0.710 69 Å). The crystal quality was tested by rotation photographs along the three crystallographic directions of the related perovskite-type lattice, and by performing ω scans on selected Bragg reflections. The sample showed sharp peaks with a full width at half maximum of about 0.1° for all reflections, which is equal to the experimental resolution. Hexagonal lattice parameters for the rhombohedral lattice were refined against the measured setting angles of 25 reflections with 2θ in the range 45°–60°, and measured in four different orientations.[16] Lattice parameters were obtained on cooling at 18 selected temperatures in the range $188.9 < T < 295$ K (Fig. 1). The cooling of the sample was achieved by a nitrogen gas stream using the FR558SH Nonius cryostat. At each temperature about 30 min was allowed in order to equilibrate the crystal temperature.

Integrated intensities of Bragg reflections were collected by ω-2θ scans in a half sphere up to $\sin(\theta)/\lambda = 1.07$ Å^{-1} at 12 selected temperatures. Data reduction was performed by HELENA software, while the absorption correction was achieved by refining the crystal shape with HABITUS software from ψ scans measured for 35 Bragg reflections at room temperature.[17,18] Each data set contained approximately 2640 reflections, which were averaged in the Laue symmetry $\bar{3}m$ toward 420 unique reflections. These data sets were used for the structure refinements (Table I). Among the unique reflections about 250 belong to the perovskite lattice and all of them are observed [$I > 3\sigma(I)$]. Superlattice reflections reflect the rhombohedral distortion of the crystal structure, and only 60 out of the 170 superlattice reflections were observed.

Structure refinements have been performed with the computer program JANA2000.[19] A starting model within the space group $R\bar{3}c$ has been taken from the literature,[3] and refinements proceeded smoothly toward excellent fits to the data. X-ray intensity data are not suitable for a determination of the relative site occupancies of La and Ba, because these elements differ by one electron only (57 and 56 electrons, respectively). Therefore, the La to Ba ratio has been fixed to 0.815:0.185, in agreement with the chemical analysis. An excellent fit to the diffraction data has been obtained, as expressed by R values of about 0.8% for all data sets. The high quality of the refinements is testified by the very small standard uncertainties on the parameters of the structural models (Table I). Structural data at room temperature from Rietveld refinements against neutron powder diffraction data on $La_{0.8}Ba_{0.2}MnO_3$ gave standard deviations of the thermal parameters that were five times higher than those found here.[3] Parameters of the structure models providing the best fit to the diffraction data at each temperature are summarized in Table I.

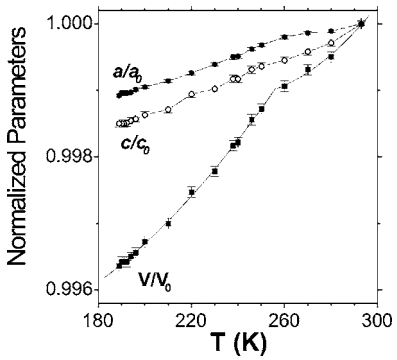

FIG. 1. Temperature dependence of the lattice parameters and unit cell volume normalized to their values a_0, c_0, and V_0 at $T = 295$ K (see Table I). The rhombohedral lattice constants are listed in Table I and they relate to hexagonal lattice constants as $a_R = \sqrt{3a^2+c^2}/3$, $\cos\alpha_R = (2c^2-3a^2)/(2c^2+6a^2)$. A change of the slope of the temperature dependence of V/V_0 occurs at $T_{cs} = 256$ K, as determined from the intersection of two second-order polynomial curves, which have been fitted to the experimental data in the ranges of temperatures $260 \leq T \leq 295$ K and $245.9 \leq T \leq 188.9$ K, respectively.

III. DISCUSSION

A. Crystal structure

The crystal structures of distorted perovskite-type compounds $La_{1-x}M_xMnO_3$ (M=Sr, Ca, Ba) are well known. They are made up of corner-sharing MnO_6 octahedra with La and M cations located in cavities with 12-fold coordination by oxygen (Fig. 2). According to previous studies, the distortions in this family of compounds are due to the interplay between the sizes of the cations and tilting of the MnO_6 octahedral groups as well as distortions of the octahedra.[20,21] In rhombohedral $R\bar{3}c$ structure the MnO_6 octahedra are trigonally distorted and tilted about [001] direction of the hexagonal unit cell ([111] direction of the pseudocubic lattice). The c lattice constant of the hexagonal unit cell is defined by the trigonal distortion, while a depends on both octahedra

TABLE I. Lattice parameters, relative atomic coordinates, and anisotropic temperature parameters U_{ij} (Å^2) obtained from the final refinements. a and c refer to the hexagonal setting and a_R and α_R refer to the rhombohedral setting of the rhombohedral lattice. Mn, (La or Ba), and O atoms are located at the sites $6b$ (0,0,0), $6a$ (0,0,1/4), and $18e$ $(0,y,1/4)$, respectively. Anisotropic temperature parameters are refined for all atoms. Standard uncertainties are given in parentheses.

Temperature (K)	188.9	190.1	191	192.2	194	196.1	200	220	237.9	245.9	260	295
a (Å)	5.5516(1)	5.5518(1)	5.5518(2)	5.5518(1)	5.5519(1)	5.5521(1)	5.5523(1)	5.5535(1)	5.5548(2)	5.5555(1)	5.5565(1)	5.5576(1)
c (Å)	13.4390(5)	13.4390(5)	13.4390(6)	13.4392(5)	13.4395(4)	13.4399(4)	13.4408(5)	13.4449(5)	13.4480(6)	13.4499(6)	13.4518(5)	13.4592(5)
V (Å^3)	358.71(2)	358.73(2)	358.73(2)	358.73(2)	358.76(1)	358.78(2)	358.84(2)	359.11(2)	359.36(2)	359.50(2)	359.68(2)	360.02(2)
a_R (Å)	5.5083(2)	5.5083(2)	5.5083(2)	5.5084(2)	5.5085(2)	5.5087(2)	5.5090(2)	5.5105(2)	5.5118(2)	5.5125(2)	5.5134(2)	5.5157(2)
α_R (deg)	60.521(3)	60.523(3)	60.523(3)	60.522(3)	60.522(3)	60.522(3)	60.521(3)	60.517(3)	60.517(3)	60.517(3)	60.518(3)	60.503(3)
U_{11}(Mn)	0.00283(10)	0.00302(8)	0.00293(7)	0.00302(7)	0.00287(7)	0.00293(7)	0.00295(6)	0.00313(6)	0.00337(5)	0.00350(5)	0.00382(7)	0.00454(6)
U_{33}(Mn)	0.0030(1)	0.0032(1)	0.0030(1)	0.0032(1)	0.0032(1)	0.0033(1)	0.0032(1)	0.0036(1)	0.0038(1)	0.0040(1)	0.0042(1)	0.0051(1)
U_{11}(La or Ba)	0.00466(8)	0.00454(5)	0.00448(4)	0.00456(5)	0.00446(4)	0.00452(4)	0.00457(4)	0.00492(4)	0.00526(3)	0.00541(3)	0.00581(4)	0.00672(4)
U_{33}(La or Ba)	0.00440(9)	0.00441(6)	0.00418(5)	0.00436(6)	0.00435(6)	0.00436(6)	0.00434(5)	0.00489(5)	0.00524(4)	0.00545(4)	0.00578(5)	0.00713(5)
y(O)	0.4527(3)	0.4528(3)	0.4529(2)	0.4528(3)	0.4528(3)	0.4532(3)	0.4531(2)	0.4528(2)	0.4529(2)	0.4528(2)	0.4528(3)	0.4526(3)
U_{11}(O)	0.0101(5)	0.0101(4)	0.0100(4)	0.0096(4)	0.0103(4)	0.0107(4)	0.0113(4)	0.0123(4)	0.0129(3)	0.0138(4)	0.0145(5)	0.0157(5)
U_{22}(O)	0.0146(3)	0.0142(3)	0.0142(3)	0.0141(3)	0.0142(3)	0.0141(3)	0.0142(2)	0.0146(2)	0.0153(2)	0.0158(2)	0.0165(3)	0.0175(3)
U_{33}(O)	0.0132(5)	0.0127(5)	0.0130(4)	0.0138(4)	0.0136(4)	0.0132(4)	0.0129(4)	0.0144(4)	0.0152(3)	0.0156(4)	0.0169(5)	0.0180(5)
U_{13}(O)	0.0040(4)	0.0036(4)	0.0041(4)	0.0044(4)	0.0045(4)	0.0041(4)	0.0044(3)	0.0049(3)	0.0046(3)	0.0047(3)	0.0054(4)	0.0048(4)
Measured reflections	2638	2637	2237	2642	2646	2647	2637	2645	2640	2640	2650	2649
Obs/all reflections	1564/2335	1603/2333	1355/1969	1565/2339	1569/2343	1575/2342	1558/2333	1541/2341	1541/2337	1521/2337	1524/2346	1475/2345
Unique obs/all reflections	324/419	327/419	318/420	324/420	320/420	321/420	322/419	312/420	311/420	307/420	308/421	292/421
R_{int}(obs/all)	0.032/0.033	0.030/0.031	0.025/0.026	0.025/0.026	0.024/0.025	0.025/0.025	0.024/0.025	0.025/0.026	0.023/0.024	0.023/0.024	0.027/0.028	0.025/0.027
R(obs/all)	0.010/0.018	0.009/0.015	0.008/0.014	0.008/0.015	0.008/0.015	0.008/0.014	0.009/0.014	0.008/0.014	0.007/0.013	0.007/0.013	0.008/0.015	0.008/0.018
wR(obs/all)	0.017/0.020	0.018/0.020	0.013/0.016	0.015/0.018	0.014/0.017	0.014/0.018	0.013/0.016	0.013/0.015	0.010/0.013	0.011/0.014	0.014/0.017	0.012/0.015

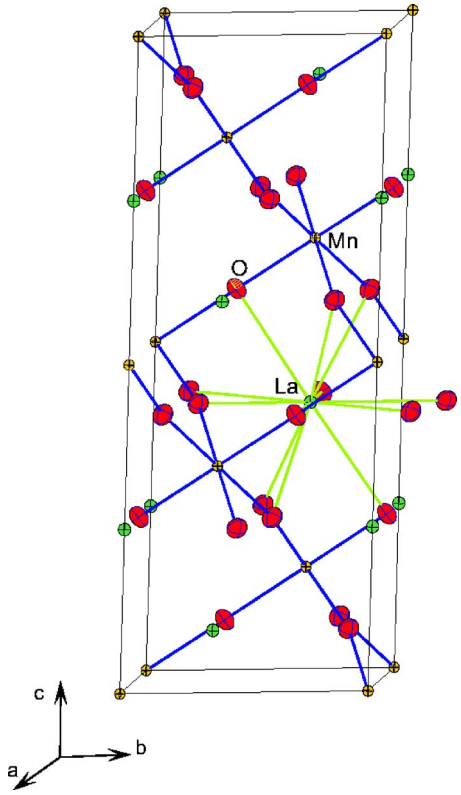

FIG. 2. (Color online) Perspective view of the crystal structure of $La_{0.815}Ba_{0.185}MnO_3$ approximately along [1 0 0]. The three longest and the three shortest La-O distances are alternated in a plane perpendicular to **c** while the six intermediate La-O distances are above and below this plane.

distortion and tilting (Fig. 2). The octahedra tilting and distortion divide the 12 La-O bonds into three groups with different bond lengths. The three longest and three shortest distances are found for three La-O contacts each that are in a plane perpendicular to **c**. The six oxygen atoms at intermediate distance from La are above and below this plane (Fig. 2). Structure refinements have provided values for all structural parameters at 12 different temperatures. Standard uncertainties of the long and short La-O bonds are one order of magnitude higher than standard uncertainties of the intermediate La-O bond, because the former have a larger dependence on the *y* coordinate of oxygen, which is the only refinable atomic coordinate in the rhombohedral structure model.

B. Magnetic phase transition

Thermal expansion is found to be slightly anisotropic within the investigated range of temperatures (Fig. 1). The temperature dependence of the volume of the unit cell changes slope at $T_{cs} \approx 256$ K. This temperature coincides with the magnetic transition temperature of $T_c \approx 251$ K within the accuracy of the present experiment. The thermal expansion coefficient of the ferromagnetic phase is found to be larger than the coefficient of the high-temperature paramagnetic phase. The effect of the PMI→FMM transition on the thermal evolution of the lattice parameters is much more pronounced in $La_{0.815}Ba_{0.185}MnO_3$ (Fig. 1) than it has been reported for rhombohedral $La_{0.815}Sr_{0.185}MnO_3$,[14] although Fig. 11 in Ref. 14 could also be interpreted towards a change of slope of the temperature dependence of *a*.

Discontinuities in the thermal evolution of the lattice parameters have been reported for the PMI→FMM phase transitions in several orthorhombic La manganites. This effect has been attributed to the absence of metallic conductivity and the concomitant presence of incoherent Jahn-Teller (JT) distortions in the high-temperature phase, which would disappear in the metallic low-temperature phase.[10,11,22] Orthorhombic $La_{0.875}Sr_{0.125}MnO_3$ exhibits a PMI→FMI transition, at which a change of slope rather than a discontinuity has been reported for the thermal evolution of the lattice parameters. This different behavior has been attributed to the insulating character of both paramagnetic and ferromagnetic phases of this compound as opposed to the low-temperature FMM state of the other compounds.[13]

This explanation does not apply to $La_{0.815}Ba_{0.185}MnO_3$ which is metallic at low temperatures, and shows a change of slope in the temperature dependence of the lattice parameters (Fig. 1). Instead, we believe that the different symmetries of the rhombohedral and orthorhombic phases might be at the origin of their different behaviors (change of slope versus discontinuity). Coherent JT distortions are forbidden by symmetry in rhombohedral structures, and modifications to the coherent JT distortions of the MnO_6 octahedral groups cannot occur in $La_{0.815}Ba_{0.185}MnO_3$, as they have been found to be important in the orthorhombic La manganites.

In agreement with this interpretation, the anisotropic displacement parameters (ADPs) such as temperature parameters and the Debye-Waller factor of oxygen display an anomalous reduction on cooling through T_c, while the smooth thermal evolution of the ADPs of La and Mn is not interrupted by the magnetic transition (Fig. 3). The discontinuity of the thermal evolution of the ADP of oxygen applies equally to its components parallel (U_{par}) and perpendicular (U_{perp}) to the direction of the Mn-O bond. It indicates a reduced incoherent JT distortion of the MnO_6 octahedra below T_c. JT distortions have been associated with charge localizations that are responsible for high electrical resistivities.[14] Reduced incoherent JT distortions thus explain the metallic character of the FMM state below T_c.

Significant anomalies at T_c are not found for the volume (V_{MnO_6}) of the MnO_6 coordination polyhedron (Fig. 4) or for the O-Mn-O bond angle (Fig. 5). These results indicate that the PMI→FMM transition is not accompanied by a change of shear distortions of the MnO_6 octahedra,[21] while coherent JT distortions are forbidden by symmetry. The thermal evolution of the Mn-O bond length changes slope at T_c (Fig. 6), but this effect is much smaller than the effect reported for orthorhombic manganites.[23]

Small changes of slopes at T_c are observed for the thermal evolution of the three shortest La-O bond lengths as well as for the volume of the LaO_{12} coordination polyhedron (Figs. 6 and 4). This behavior reflects the anomalies in the lattice parameters and unit cell volume, because *a* is equal to the sum of the lengths of the longest and shortest La-O bonds.[20,24] La-O bond lengths are intimately related to the tilt of the MnO_6 octahedral groups.

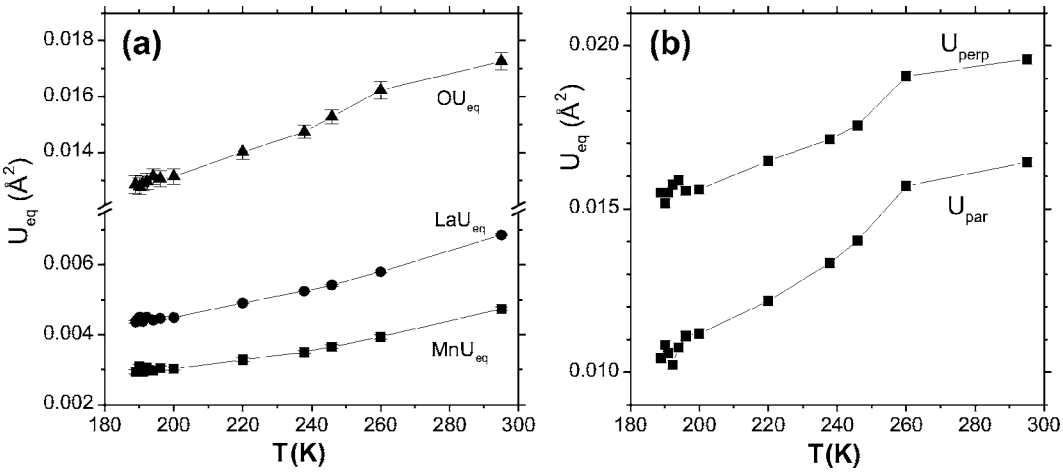

FIG. 3. Temperature dependence of atomic displacement parameters (ADPs). (a) Equivalent isotropic ADPs for all atoms; (b) components of the ADP tensor of oxygen, with U_{par} representing the component along the Mn-O bond, and U_{perp} representing the mean value of the ADP tensor within the plane perpendicular to the Mn-O bond.

C. Rhombohedral to monoclinic transition

At T_S=187.1(3) K, $La_{0.815}Ba_{0.185}MnO_3$ exhibits a first-order phase transition toward a state with monoclinic symmetry.[5] Similar transitions in other La manganites have been interpreted as rhombohedral to orthorhombic transitions.[14] Indeed, the diffracted intensities of $La_{0.815}Ba_{0.185}MnO_3$ below T_S can be interpreted by an orthorhombic structure model in very good approximation, but a careful analysis of the superlattice reflections has unambiguously determined the monoclinic space group $I2/c$.[5]

Precursor effects are visible as anomalous variations of several structural parameters within the rhombohedral phase close to T_S (Figs. 4–7). The Mn-O bond length reaches a minimum at 196 K and remains constant down to 188.9 K, with a value of 1.9726(2) Å that extrapolates well toward $\langle d(\text{Mn-O})\rangle_{av}$=1.973(2) Å in the monoclinic phase at T =160 K [Fig. 6(e)].[5] The same observation can be made for the polyhedral volume of MnO_6, with values of 10.23(1) $Å^3$ in the rhombohedral phase and of 10.24(3) $Å^3$ in the monoclinic phase [Fig. 4(a)].[5] The bond angle O-Mn-O remains constant down to T_S at a value of 91.0°, while the average value within the monoclinic phase is 90.30° (Fig. 5).[5] Together these results indicate that the shear distortion of the MnO_6 octahedron in the rhombohedral phase is replaced by a small Jahn-Teller-type distortion in the monoclinic phase.[21] The driving force for the rhombohedral to monoclinic phase transition might thus be the higher stability of JT-distorted MnO_6 octahedral groups as opposed to the shear-distorted octahedral groups in this compound.

The tilt angle of the MnO_6 groups decreases from T_c down to 196 K [Fig. 7(a)]. At this temperature it reaches a minimum, while it increases on further cooling down to T_S. As a consequence of the rhombohedral symmetry, this variation of tilting of MnO_6 groups implies that the shortest La-O bond decreases while the longest La-O bond must increase on cooling from 196 K down to T_S, as is indeed observed [Figs. 6(f) and 6(h)]. The longest and shortest La-O bonds each correspond to two independent bonds in the monoclinic phase, while the six La-O bonds of intermediate length split into one short bond, one long bond, and one bond of intermediate length in the monoclinic phase.[5] The average values of bond lengths in the monoclinic phase compare well with the values in the rhombohedral phase [$\langle d(\text{La-O})_{short}\rangle_{av}$=2.552 Å, $\langle d(\text{La-O})_{intermediate}\rangle_{av}$=2.781 Å, and $\langle d(\text{La-O})_{long}\rangle_{av}$=2.972 Å]. In agreement with the observed precursor effects, the shortest La-O bond in the monoclinic structures[5] (2.457 Å) can be obtained by following the downward trend of the shortest La-O bond within the rhombohedral phase (Fig. 6). Similarly, the longest La-O bond in the rhombohedral phase can be extrapolated toward an even longer bond in the monoclinic phase (3.053 Å).[5] An alternative proposal for the driving force of the phase transition thus is a more stable environment of La as it can be achieved in the monoclinic phase.

The pattern of tilts of MnO_6 octahedral groups is dictated by symmetry, and it thus is different in the low- and high-temperature structures. One crystallographically independent tilt angle exists in $R\bar{3}c$ symmetry (tilting about [001] of the

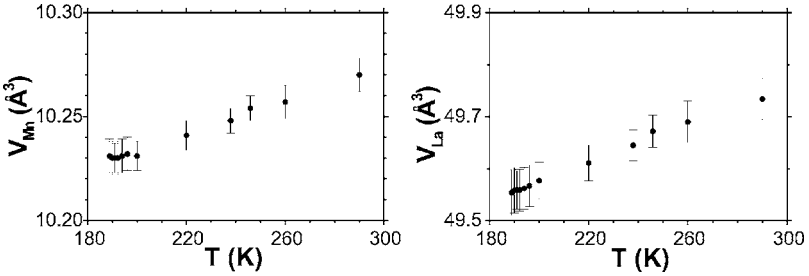

FIG. 4. Temperature dependencies of the MnO_6 and LaO_{12} polyhedral volumes for $La_{0.815}Ba_{0.185}MnO_3$.

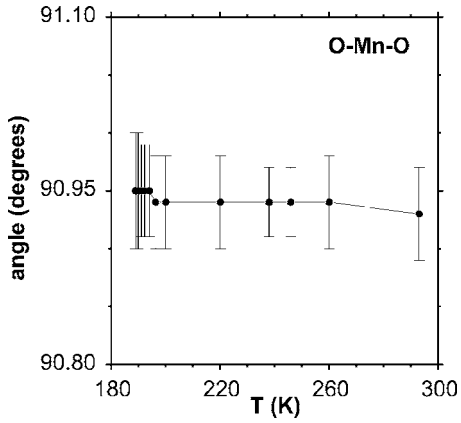

FIG. 5. Temperature dependence of the O-Mn-O bond angle for $La_{0.815}Ba_{0.185}MnO_3$.

hexagonal lattice [Fig. 7(a)]),[25] while in the monoclinic structure the tilting could be described by two independent rotations about axes with directions close to [100] and [001] of the monoclinic lattice. These entirely different patterns are illustrated by the quite different values of the two tilt angles, as they have been determined for the monoclinic phase ($\varphi = 0.22°$ and $\theta = 9.58°$), and as they can be computed for the monoclinic setting of the rhombohedral structure [Fig. 7(b)].[26] On cooling the tilt angle of the rhombohedral phase decreases smoothly. Just above the structural phase transition it begins to increase rapidly and can be extrapolated toward the θ tilting value of the monoclinic structure. The small φ tilting angle in monoclinic structure allows this first-order rhombohedral-monoclinic structural phase transition interpret as a change of tilting axis direction from [001] of hexagonal lattice toward [100] direction of the monoclinic lattice.

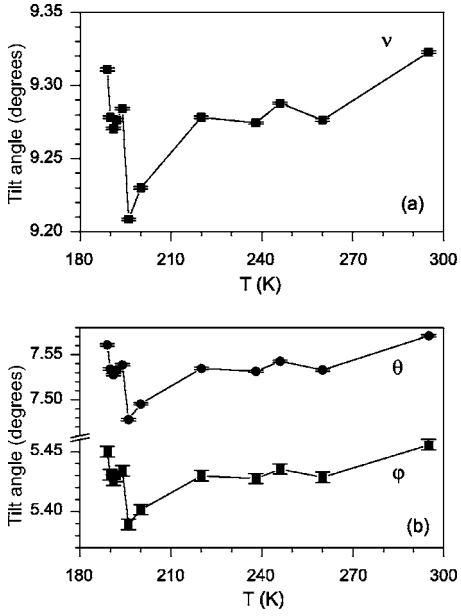

FIG. 7. (a) Temperature dependence of the tilt angle of rhombohedral $La_{0.815}Ba_{0.185}MnO_3$. (b) Tilt in the rhombohedral phase (ν) decomposed into two tilt angles of the monoclinic setting of the lattice (φ and θ) (Ref. 26).

IV. CONCLUSIONS

Crystal structures of $La_{0.815}Ba_{0.185}MnO_3$ have been determined by accurate single-crystal x-ray diffraction for 12 selected temperatures within the rhombohedral phase between $T_S = 188.9$ K and room temperature.

Thermal expansion is found to be discontinuous at the paramagnetic to ferromagnetic phase transition at $T_c = 251$ K, with the larger value for the thermal expansion co-

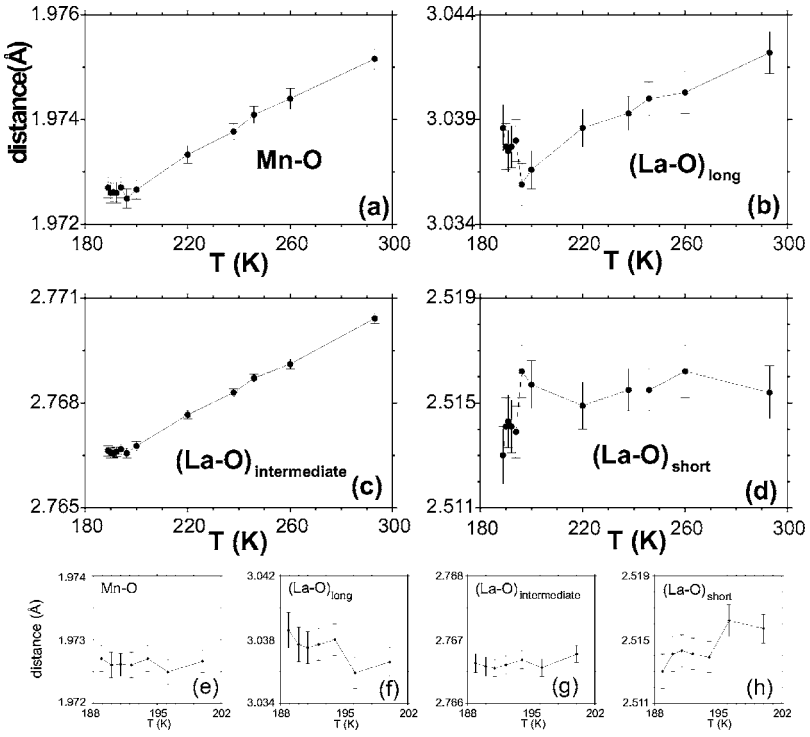

FIG. 6. Temperature dependence of bond lengths in $La_{0.815}Ba_{0.185}MnO_3$. (a) Mn-O bond; (b) La-$O_{long}$; (c) La-$O_{intermediate}$; (d) La-$O_{short}$. (e)–(h) show enlargements of the region near T_S.

efficient of the low-temperature ferromagnetic phase (Fig. 1). A major effect of the magnetic transition on the crystal structure is an anomalous decrease of both the parallel and perpendicular components of the ADPs (temperature tensors) of the oxygen atoms. This indicates that the incoherent distortions of the MnO_6 octahedral groups are smaller in the magnetically ordered phase than they are in the paramagnetic phase.[14] Essentially different structural behavior is found in the vicinity of T_c for rhombohedral $La_{0.815}Ba_{0.185}MnO_3$ and several orthorhombic La manganites.[10] These differences can be attributed to the different crystal symmetries, which prevent coherent JT distortions in $R\bar{3}c$, and thus prevent modifications to the structural distortions as they have been found to be important in the orthorhombic La manganites.[10]

Precursor effects close to the rhombohedral to monoclinic phase transition have been found to involve both the shapes and the tilts of the MnO_6 octahedra as well as the coordination polyhedron of La. The anomalous behavior near T_S extrapolates well to values of the parameters found in the monoclinic phase.[5] Both the replacement of shear distortion by JT-type distortion of the MnO_6 groups and a more stable environment of La in the monoclinic structure may contribute to the driving force for the rhombohedral to monoclinic structure phase transition.

ACKNOWLEDGMENTS

Detlef Krauße and the Bayerisches Geoinstitut (Bayreuth) are thanked for supplying the electron microprobe measurement. Financial support by the German Science Foundation (DFG) is gratefully acknowledged.

*Electronic address: smash@uni-bayreuth.de
URL: www.crystal.uni-bayreuth.de

[1] G. H. Jonker and J. H. van Santen, Physica (Amsterdam) **16**, 337 (1950).
[2] J. H. van Santen and G. H. Jonker, Physica (Amsterdam) **16**, 599 (1950).
[3] B. Dabrowski, K. Rogacki, X. Xiong, P. W. Klamut, R. Dybzinski, J. Shaffer, and J. D. Jorgensen, Phys. Rev. B **58**, 2716 (1998).
[4] V. E. Arkhipov, N. G. Bebenin, V. P. Dyakina, V. S. Gaviko, A. V. Korolev, V. V. Mashkautsan, E. A. Neifeld, R. I. Zainullina, Y. M. Mukovskii, and D. A. Shulyatev, Phys. Rev. B **61**, 11229 (2000).
[5] N. Rotiroti, R. Tamazyan, S. van Smaalen, and Y. Mukovskii, Acta Crystallogr., Sect. C: Cryst. Struct. Commun. **61**, i83 (2005).
[6] R. Tamazyan, S. van Smaalen, A. Arsenov, and Y. Mukovskii, Phys. Rev. B **66**, 224111 (2002).
[7] J. L. Ju, Y. S. Nam, J. E. Lee, and H. S. Shin, J. Magn. Magn. Mater. **219**, 1 (2000).
[8] J. Zhang, H. Tanaka, T. Kanki, J.-H. Choi, and T. Kawai, Phys. Rev. B **64**, 184404 (2001).
[9] P. G. Radaelli, D. E. Cox, M. Marezio, S.-W. Cheong, P. E. Schiffer, and A. P. Ramirez, Phys. Rev. Lett. **75**, 4488 (1995).
[10] P. G. Radaelli, M. Marezio, H. Y. Hwang, S.-W. Cheong, and B. Batlogg, Phys. Rev. B **54**, 8992 (1996).
[11] J. M. De Teresa, C. Ritter, M. R. Ibarra, P. A. Algarabel, J. L. García-Muñoz, J. Blasco, J. García, and C. Marquina, Phys. Rev. B **56**, 3317 (1997).
[12] Q. Huang, A. Santoro, J. W. Lynn, R. W. Erwin, J. A. Borchers, J. L. Peng, K. Ghosh, and R. L. Greene, Phys. Rev. B **58**, 2684 (1998).
[13] D. N. Argyriou, J. F. Mitchell, C. D. Potter, D. G. Hinks, J. D. Jorgensen, and S. D. Bader, Phys. Rev. Lett. **76**, 3826 (1996).
[14] B. Dabrowski, X. Xiong, Z. Bukowski, R. Dybzinski, P. W. Klamut, J. E. Siewenie, O. Chmaissem, J. Shaffer, C. W. Kimball, J. D. Jorgensen, and S. Short, Phys. Rev. B **60**, 7006 (1999).
[15] Y. Mukovskii, V. Arkhipov, A. Arsenov, N. Bebenin, V. Dyakina, V. Gaviko, A. Korolev, S. Karabashev, V. Mashkautsan, E. Neifeld, D. Shulyatev, and R. Zainullina, J. Alloys Compd. **326**, 108 (2001).
[16] Computer code CAD-4 (Enraf-Nonius, Delft, The Netherlands, 1989).
[17] A. L. Speck, Computer code HELENA (University of Utrecht, The Netherlands, 1997).
[18] W. Herrendorf and H. Bärnighausen, Computer code HABITUS (University of Karlsruhe, Karlsruhe, Germany, 1997).
[19] V. Petriceck, M. Dusek, and L. Palatinus, Computer code JANA2000 (Institute of Physics, Prague, Czech Republic, 2000).
[20] J. B. Goodenough, Rep. Prog. Phys. **67**, 1915 (2004).
[21] A. Arulraj, R. E. Dinnebier, S. Carlson, M. Hanfland, and S. van Smaalen, Phys. Rev. Lett. **94**, 165504 (2005).
[22] M. R. Ibarra, P. A. Algarabel, C. Marquina, J. Blasco, and J. García, Phys. Rev. Lett. **75**, 3541 (1995).
[23] P. G. Radaelli, G. Iannone, M. Marezio, H. Y. Hwang, S.-W. Cheong, J. D. Jorgensen, and D. N. Argyriou, Phys. Rev. B **56**, 8265 (1997).
[24] T. B. Žunić and I. Vicković, J. Appl. Crystallogr. **29**, 305 (1996).
[25] A. M. Glazer, Acta Crystallogr., Sect. B: Struct. Crystallogr. Cryst. Chem. **28**, 3384 (1972).
[26] The angle θ denotes rotation of the MnO_6 octahedron about an axis parallel to an O2-O2 edge of the octahedron (equatorial oxygen atoms) and going through the Mn atom. The angle ϕ describes rotation about an axis perpendicular to the **a**,**b** plane of the monoclinic unit cell (Ref. 5). Zero tilt ($\theta=\phi=0$) is defined as the fictitious structure with angles Mn-O2-Mn equal to 180°.